

Heusler 4.0: Tunable Materials

Lukas Wollmann,¹ Ajaya K. Nayak,^{1,2}
Stuart S. P. Parkin,² and Claudia Felser¹

¹Max-Planck-Institut für Chemische Physik fester Stoffe, Dresden, Germany, D-01187

²Max-Planck-Institut für Mikrostruktur Physik, Halle, Germany, D-06120

xxxxxx 0000. 00:1–28
Copyright © 0000 by Annual Reviews.
All rights reserved

Keywords

half-metallic ferromagnetism, *half*-Heusler compounds, tetragonal Heusler compounds, topological materials, Weyl semi-metals, non-collinear magnetic order

Abstract

Heusler compounds are a large family of binary, ternary and quaternary compounds that exhibit a wide range of properties of both fundamental and potential technological interest. The extensive tunability of the Heusler compounds through chemical substitutions and structural motifs makes the family especially interesting. In this article we highlight recent major developments in the field of Heusler compounds and put these in the historical context. The evolution of the Heusler compounds can be described by four major periods of research. In the latest period, Heusler 4.0 has led to the observation of a variety of properties derived from topology that includes: topological metals with Weyl and Dirac points; a variety of non-collinear spin textures including the very recent observation of skyrmions at room temperature; and giant anomalous Hall effects in antiferromagnetic Heuslers with triangular magnetic structures. Here we give a comprehensive overview of these major achievements and set research into Heusler materials within the context of recent emerging trends in condensed matter physics.

Contents

1. HEUSLER 1.0 – TURNING NON-MAGNETIC ELEMENTS INTO FERROMAGNETIC MATERIALS	3
2. HEUSLER 2.0 – HALF METALLICITY	6
2.1. Co-based Half-metallic Ferromagnets	6
2.2. Mn-based Half-metallic Ferrimagnets	7
2.3. Compensated Ferrimagnets	9
2.4. Spin-gapless Semiconductors	11
3. HEUSLER 3.0 – UNIAXIAL HEUSLER COMPOUNDS AND NON-COLLINEAR SPIN STRUCTURES	12
3.1. Tetragonal Heusler Compounds for Spin-Transfer Torque	12
3.2. Tetragonal Compensated Ferrimagnetic Heusler Compounds	13
3.3. Non-collinear magnetic structure	14
4. HEUSLER 4.0 – TOPOLOGICAL HEUSLER COMPOUNDS	17
4.1. GdPtBi – a Weyl-Semimetal in a magnetic field	18
4.2. Co ₂ TiSn – a magnetic, centrosymmetric Weyl semimetal	19
5. SUMMARY	22

1. HEUSLER 1.0 – TURNING NON-MAGNETIC ELEMENTS INTO FERROMAGNETIC MATERIALS

The history of Heusler compounds dates back to 1903, the year of Friedrich Heusler's seminal contribution (1, 2) in the *Verhandlungen der deutschen physikalischen Gesellschaft*, where he announced the discovery of a ferromagnetic material at room temperature, that is surprisingly formed from the elements, Cu, Mn, and Al that show no magnetism at room temperature. Later ferromagnetism was found in other compounds formed from Cu, and Mn but with several other elements $Z = \text{Sb, Bi, Sn}$. Today, this perhaps does not seem so surprising especially since the concepts of antiferromagnetism and ferrimagnetism were introduced by Louis Néel in the 1930s-1940s (3, 4). However, these phenomena were unknown in 1903, which made Heusler's work a major finding. The structure of the compound that Heusler prepared was also unknown in 1903, although Heusler realized that a chemical compound must have been formed. He thus anticipated what is today widely understood and accepted: Heusler compounds form a special class of materials, that are located at the border between compounds and alloys, and which combine features of both, namely, the chemical stability of a covalent lattice from which the Heusler compound is constructed, while single sites within the lattice can be substituted by different species and thereby behave as single-site alloys. In a nutshell, covalency and tunability best describe the uniqueness of this materials class. It was not until 1934 that Otto Heusler, Heusler's son (5), and Bradley (6), determined the crystal structure of Cu_2MnAl . Otto Heusler noted the possibility of another type of crystalline order that is nowadays termed an *inverse/inverted* Heusler compound with the spacegroup T_2^d (5) in the notation of Schoenflies or 216 in today's space group classification. The Heusler structure can be described as intertwined cubic and rocksalt lattices, or as four interpenetrating *fcc* sublattices, of which two are formed from the same element.

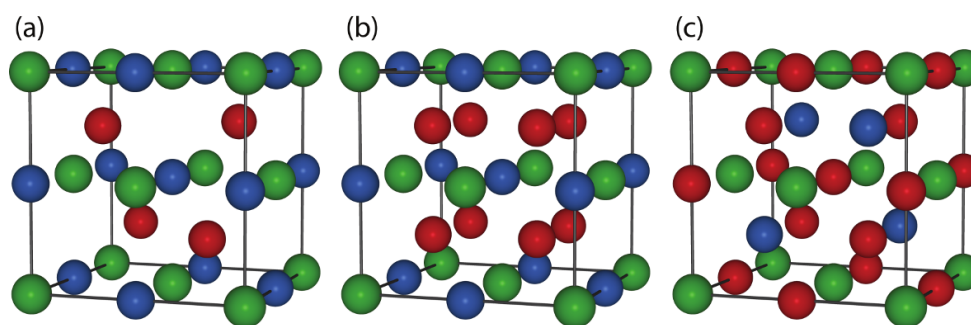


Figure 1

(Color online) The three prototypical Heusler structures, wherein X atoms are represented by red spheres, Y atoms by blue/light blue and Z atoms by green spheres: (a) *half*-Heusler, (b) *regular* Heusler, (c) *inverse* Heusler structure.

Shortly after Heusler's discovery, Nowotny and Juza, published results on a different group of materials, all main-group element compounds, namely LiMgAs (Nowotny) and CuMgAs (Juza), that are nowadays referred to as Nowotny-Juza-Phases. The connection between the Nowotny-Juza phases and the Heusler compounds, was established by L. Castelliz, who first synthesized NiMnSb (7, 8), as part of the compositional series $\text{Ni}_{2-x}\text{MnSb}$ ($0 \leq x \leq 1$). NiMnSb and the Nowotny-Juza-Phases are now described as *half*-Heusler compounds in

which one of the 4 *fcc* sub-lattices of the *full* Heusler is empty. By filling this 4th sub-lattice a series of compounds can be formed between *half* and *full* Heuslers, which we can describe as XYZ and X_2YZ , respectively, where X , Y are transition metal elements and Z is a main group element. The *full* Heusler compounds have several variants including the *inverse* structure in which one of the X elements is swapped with Y , and quaternary Heuslers in which one of the X is replaced by a 4th distinct element.

Type	Order	$4d^{\text{HC}}$	$4c$	$4b$	$4a$	Example
Fluorite	C1	A		E	E	$\text{Ca}^{\text{HC}}\text{F}_2$
Juza	C1_b	E		A	A'	LiMgN^{HC}
Nowotny	C1_b	E		T	A	$\text{MgAgAs}^{\text{HC}}$
Nowotny	C1_b	T		A	E	$\text{MgCu}^{\text{HC}}\text{Sb}$
<i>Half</i> – Heusler	C1_b	T		T'	E	$\text{MnCu}^{\text{HC}}\text{Sb}$
<i>Full</i> – Heusler	L2_1	T	T	T'	E	$\text{Cu}_2^{\text{HC}}\text{MnAl}$
<i>Inverse</i> – Heusler	X_a	A	T	A	E	Li_2AgSb

Table 1 The different site occupations as they are found in cubic Heusler and Heusler-related-structures. See also (9).

Thus, it is clear that the Heusler name now refers to a broad and extensive family of compounds. Furthermore, all of these variants can be subjected to various structural distortions including a tetragonal elongation or compression along one of the cubic crystal axes, or a distortion along the $[111]$ direction that leads to an hexagonal structure (9). Finally, superstructures are sometimes found that can arise from chemical ordering in non-stoichiometric compounds or from modulation of the structure and structural phase transitions, for example, in the case of shape memory alloys. The key differences between these various Heusler compounds are highlighted in Table 1.

The three main prototypical Heusler stoichiometric, chemically ordered structural types, namely the *half*, *regular* and *inverse* are shown in Figure 1.

Early reports on Heusler phases (10) appear in the context of $X_2\text{MnZ}$ alloys, where $X = \text{Ni}, \text{Pd}, \text{Au}$ and $Z = \text{Al}, \text{Si}, \text{Ga}, \text{Ge}, \text{In}, \text{Sn}, \text{Sb}$, with a particular focus on their chemical and magnetic order, and an ordering transition that can be induced by composition or by temperature, or pressure. (7, 11, 12). Remarkably, a ferro- to antiferromagnetic transition was observed in $\text{Pd}_2\text{MnIn}_{1-x}\text{Sn}_x$ (13). Webster and co-workers were the first to explore the magnetic properties of the Co_2MnZ compounds, which they stated were quite different from previously studied Heuslers, as they incorporate elements other than Mn that carry a substantial local magnetic moment (10). They did not anticipate the great interest of the scientific community in these materials that has occurred over the past decade.

It is worth mentioning that cousins of the original Heusler-type were found in the 1960–1970s at the IBM Research Laboratory, San Jose (CA). Jim Suits explored the Rh_2 -based Heusler compounds, and found a structural transformation at temperatures of about 700–800 K, with a very large deformation amplitude $\varepsilon = c_{\text{tet}}(c_{\text{cub}} - 1)$ of about 17% which is of the same size as the Mn^{3+} Jahn-Teller-ion containing spinels (14, 15). Some of these compounds were non-magnetic and some antiferromagnetic, and some showed tetragonally distorted derivatives which have become of considerable interest today.

It was not until much later, that the Co_2 -based Heusler compounds received renewed at-

tention in the context of half-metallic ferromagnetism (HMF). Half-metallic ferromagnets, exhibit metallic behavior in one spin channel and an insulating behavior in the other, and thus are of great interest because they intrinsically should have fully spin polarized electronic states at the Fermi energy (16).

The first example of the Heusler HMF was first realized by de Groot *et al.* for the case of NiMnSb (17). Such materials are also of great interest for spintronic applications, for example, as magnetic electrodes in magnetic tunnel junctions. Magnetic tunnel junction are composed of two magnetic electrodes separated by a thin tunnel barrier. The current crossing the tunnel barrier from one electrode to the other depends on the magnetic configuration of the electrodes. When the moments of the two electrodes are aligned parallel to one another the current can flow easily but when the moments of the two electrodes are aligned exactly anti-parallel to one another the tunneling current will be reduced, and, for the case of HMF, should go to zero.

While semiconducting Heusler compounds are usually not magnetic, magnetism can be introduced by the introduction of *RE* elements, *RE*PtBi or Mn on the *4b* position. Whilst the Mn containing compounds become metallic, the *REYZ* remain semi-conducting due to the localization of the $4f^n$ -electrons. The semiconducting behavior of MnYZ (commonly written as YMnZ) is conserved only in one spin-channel, and therefore these compounds have been coined "half-metallic ferromagnets", in which one spin-channel exhibits semi-conducting or insulating characteristics caused by a minority gap, while the majority spin-channel is metallic. NiMnSb is of this type and has 22 valence electrons. This compound has four excess electrons as compared to the semi-conducting Heuslers that have a valence electron count of $N_V = 18$. Interestingly, these excess electrons fill one spin-channel and thereby form a spin magnetic moment of $M_{spin} = 4\mu_B$. In this way these compounds follow almost exactly the Slater-Pauling rule whereby $M_{spin} = N_V - 18$. We will return to this point later (Sec. 2.2.2). The early work on NiMnSb emphasized its magneto-optical properties that was stimulated by the large magneto-optical Kerr angle of 1.27° found in PtMnSb, one of the other early HMFs (17).

2. HEUSLER 2.0 – HALF METALLICITY

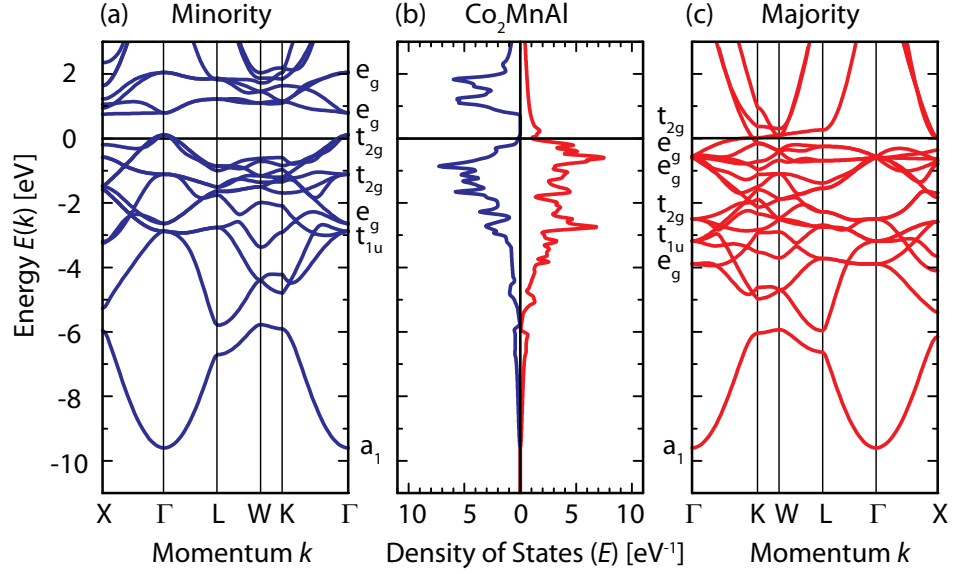


Figure 2

(Color online) Band structure of Co_2MnAl depicting the $E(k)$ dispersion relation for the minority (a) and majority (c) spin channels, together with the density of states (b)

2.1. Co-based Half-metallic Ferromagnets

It was Ishida *et al.*, who first began exploring HMF in Co_2 -based Heusler compounds, such as Co_2MnSn , Co_2TiAl , Co_2TiSn , using LDA methods to calculate their electronic structure. However, Ishida *et al.* did not obtain HMF in these compounds (18) because the LDA (19) formalism did not allow for a minority gap to open. This was later confirmed by Kübler *et al.* (20), who noted, however, that *peculiar transport properties* are to be expected for these nearly HMF-type compounds. It was in the same year, 1983, that Kübler studied the formation and coupling of the magnetic moments in Co_2MnSn and similar Co-based alloys, and remarked how their spin magnetic moments follow a linear behavior with the number of valence electrons. Kübler *et al.* quickly recognized the peculiar role of Mn in the $X_2\text{MnZ}$ type compounds. They could reproduce the ferro- to antiferromagnetic transition from Pd_2MnIn to Pd_2MnSn and elaborated on the formation of localized magnetic moments in purely itinerant magnets, triggered by the strong exchange splitting of the d -states attributed to the Mn-site. These findings were soon put into context, and chemical trends were established of which the backbone is the Slater-Pauling (SP) rule. The Slater-Pauling rule was first expressed as a function of the magnetic valence, but soon reformulated in a more general manner. Originally the SP-rule covered elements and binary alloys (21), but the extension to ternary alloys led to the wide success of the SP-rule as a very useful tool for assessing the expected magnetic moment of a ternary HMF. The Slater-Pauling rule describes the interplay of electron filling and the resulting magnetic moment. In Co-based *full*-Heusler alloys, a valence electron count of 24 leads to a zero net moment as both spin-

channels are occupied by 12 valence electrons each. Filling or depleting electrons leads to a net integer spin-moment $M = N_V - 24$.

Further contributions to the theory of Heusler alloys showed how the SP-rule could be described using molecular orbital coupling schemes and symmetry analysis. Fecher *et al.* emphasized that an upper bound of approximately $6 \mu_B$ (24) is unlikely to be exceeded, as the *s*-states which were to be populated in the majority spin-channel are strongly dispersed, which would lead to an energetically unfavorable situation. Furthermore, it could be shown that some compounds involving late transition metals $Y = \text{Cu, Zn}$, e.g. Mn_2ZnSi , do not obey the SP-rule as $M = N_V - 24$, but another situation occurs in which doubly degenerate *d*-states are shifted below a set of triply degenerate states caused by the symmetry of the crystal structure (X_a , no inversion), such that the equation $M = N_V - 28$ guides the emerging magnetic moments (23).

The Slater-Pauling rule is a simple yet powerful tool for the prediction of half-metallic ferromagnets. In principle, one would not expect a simple relationship between a compound's magnetic moment, and the critical magnetic ordering temperature, that depends sensitively on the electronic structure. In the Heisenberg picture, this depends on an atom's nearest neighbors. In Co-based Heusler compounds, a simple relationship wherein $T_C \propto M$ has been found (25). This is another beautiful example of the fundamental tunability of Heusler compounds, limited only by their chemical stability. The evolution of the Curie temperature is traced back to two competing factors in terms of the spherical approximation (SPA), namely the decreasing average exchange energy counterbalanced by an increasing total moment with increasing number of valence electrons. It was concluded that the double-/kinetic exchange mechanism of Zener provides the key concept to the understanding of the observed behavior (25, 26).

The beginning of a phase of intense research on the Heusler class of compounds that lay the foundation for the current perspective of Heusler compounds as multi-potential materials, possibly providing answers for many materials science challenges, was in the beginning of the 1980s. The use of half-metallic ferromagnets in spin-valve structures should lead to out-of-scale magnetoresistance, from which the field of spintronics received an activity boost. Spin-valve structures based on NiMnSb did not appear to be promising in the beginning so mechanisms leading to a possible suppression of the expected high TMR values were explored. By means of relativistic *first principles* calculations it was shown that spin-orbit coupling induces a finite but negligibly DOS for 3*d*-based Heusler compounds, while this effect is more severe for PdMnSb and PtMnSb . After these less successful attempts, the incorporation of Co₂-based Heusler alloys, such as $\text{Co}_2\text{Cr}_{0.6}\text{Fe}_{0.4}\text{Al}$ (27) and Co_2MnSi into spin-valve structures succeeded in delivering the expected MR-values in the range of $\text{MR} \approx 2000\%$, after many years of materials and interface engineering (28). Quite recently, in 2014, spin-polarized photoemission experiments conducted by Jourdan *et al.*, supported by theoretical calculations, provided proof of half-metallic ferromagnetism in Co₂-based Heusler alloys (in the exemplary compound Co_2MnSi) (within the experimental accuracy) (29).

2.2. Mn-based Half-metallic Ferrimagnets

In addition to NiMnSb and Co_2MnSi , Mn_2VAl has also attracted a lot of attention, as it was early identified as a HMF by numerical methods (30). Nevertheless, experimental and theoretical studies have largely focused on the Co-based compounds. Renewed interest in

the Mn-based compounds was triggered by the discovery of structurally distorted cousins of the cubic systems: namely, the tetragonally distorted Heusler compounds. The most renowned member, Mn_3Ga (31), was already studied in the 1970s, yet the potential for spintronic applications was not recognized until the late 2000s (32, 33).

The first example of a member of the Mn_2 - family is without doubt Mn_2VAl . It was synthesized by Kopp (34) and Nakamichi (35), but misinterpreted as a ferromagnet, which was later corrected by neutron diffraction measurements (36), before it was studied within the scope of half-metallicity (30). Mn-based materials received renewed attention in the late 2000s, when ferrimagnetic Heusler compounds were proposed as free-magnetic layers for spin-valve structures, such as, for example, magnetic tunnel junctions, in which a spin-polarized current is used to trigger the switching of the free-layer. For a long time Mn_2VAl was the only known member of that class until low moment magnets for spintronics/electrodes/memory received renewed attention, which led to the discovery of ferrimagnetic Heuslers with low magnetization. Further half-metallic ferrimagnetic Mn_2VZ -Heusler compounds were predicted by DFT based computations (37, 38, 39). With these compounds it was realized that Slater-Pauling behavior is possible even when the valence electron count is less than 24. Then negative moments are formally computed, which reflects the relative magnitudes of the individual sub-lattice moments, when the orientation of these sub-lattices is fixed with respect to the crystal lattice. This can lead to a compensation point, where the two sub-lattice moments are identical. When the composition is systematically varied within a given compositional series, this is particularly interesting, as the a sign change of the net magnetic moment may also give rise to a sign change in other properties.

The formation of magnetic moments on the Mn atoms at site $4b$ was explained by Kübler (20), and is found to be correct even within the Mn_2 -Heusler family. The Mn atoms at the $X(4c/4d)$ site are found to have small moments comparable to that of the Co atoms at the same positions within the Co_2 -Heusler class. A high moment, of about $3-4 \mu_B$ at site $Y(4b)$ (39) was observed from the very beginning of studies on these compounds, and was identified as a characteristic feature of the Mn-Z layer. The Mn_2 -Heuslers can also form another type of order that is today termed as *inverted*. It emphasizes the fact, that an atomic swap/exchange is observed in comparison to the prototypical Cu_2MnAl type, within which the X atoms evenly occupy the site $8c$ in the inversion symmetric spacegroup 225. Independent of these types of order, the Slater-Pauling rule remains valid even for the inverted type.

Further ferrimagnetic and possibly half-metallic systems have been studied for their magnetic ground-states, while these studies often refer to simple numerical calculations, neglecting other types of magnetic and structural order. Mn_3Ga is a material that exhibits features of *regular* X_2YZ and *inverse* $XYXZ$ ordered Heusler compounds at the same time. At first, the even distribution of Mn atoms at the $8c$ position, that resembles *regular* order in X_2YZ , while the occupation of Mn atoms of the $4b$ position is indeed a feature of *inverse* order in the Mn_2 -Heusler class, as for instance in Mn_2CoAl , where Mn and Co are located at $4d/4c$ and Mn and Al at $4b$ and $4a$. In theory Mn_3Ga crystallizes in the centrosymmetric space group 225 (prototype BiF_3) showing compensated ferrimagnetism (41). That said, it is found in various studies, that systems incorporating early transition metals as Y elements prefer the *regular* order, while choosing late transition metals the *inverse* order is preferred (42, 43, 39), where the early and late transition metals are separated by Mn. This observation is known as *Burch's rule* (42). In experimental studies bulk- Mn_3Ga has been found to stabilize in a tetragonal lattice (see Sec. 3.3.1 and 3.3.2)

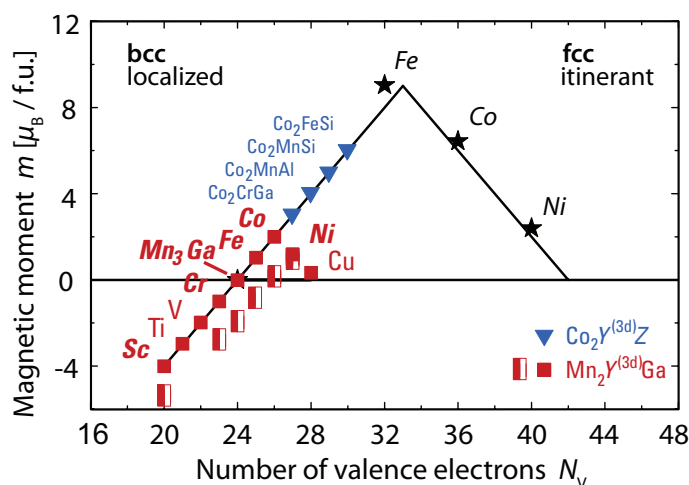


Figure 3

(Color online) Schematic representation of the Slater-Pauling behavior for a set of selected Mn_2YZ and Co_2YZ compounds. Based on Refs. (39, 40)

2.3. Compensated Ferrimagnets

Despite their potential for obtaining 100% spin polarization, HMFs typically produce large magnetic dipole fields that can hinder the performance of spintronic devices that contain them. Therefore, materials that display 100% spin polarization but with very low or, even more interestingly, zero net magnetic moment are of special interest, both technologically as well as scientifically. According to the Slater–Pauling (44, 45) rule, which, as discussed above, also describes the HMF Heuslers, the total magnetic moment (M) of the L_{21} cubic Heusler compounds is given by $M_{\text{spin}} = N_{\text{v}} - 24$, where N_{v} is the number of valence electrons. Thus, Heusler compounds with 24 valence electrons should exhibit a zero net magnetic moment. The search for compensated ferrimagnetic Heuslers with 24 valence electrons has been focussed on the Mn-based Heusler compounds since the Mn atoms sit in an octahedral environment that results in a strongly localized magnetic moment. An example of a 24 valence electron based Heusler compound is Mn_3Ga , which is predicted to display half-metallicity in the cubic L_{21} structure. Unfortunately, cubic Mn_3Ga does not exist in the bulk form due to a tetragonal distortion that destroys both the compensated magnetic state and the half-metallic behavior. Recently, it has been shown that it is possible to achieve a compensated magnetic state in cubic thin films of $\text{Mn}_2\text{Ru}_x\text{Ga}$ (46, 47). In this case, the compensated magnetic state was obtained in off-stoichiometric thin films having 21 valence electrons.

Recently, Stinshoff *et al.* have found that the cubic L_{21} compound $\text{Mn}_{1.5}\text{FeV}_{0.5}\text{Al}$ with 24 valence electrons exhibits a fully compensated ferrimagnetic state (48). As shown in Figure 4(a), $\text{Mn}_{1.5}\text{FeV}_{0.5}\text{Al}$ crystallizes in the *regular* L_{21} cubic Heusler structure with space group $Fm\bar{3}m$. Al atoms (green spheres) occupy the $4a$ position, V (grey) and MnI (red) atoms equally occupy the $4b$ position, whereas, the $8c$ position is occupied equally by MnII (green) and Fe (light yellow) atoms. A calculation of the site specific magnetic

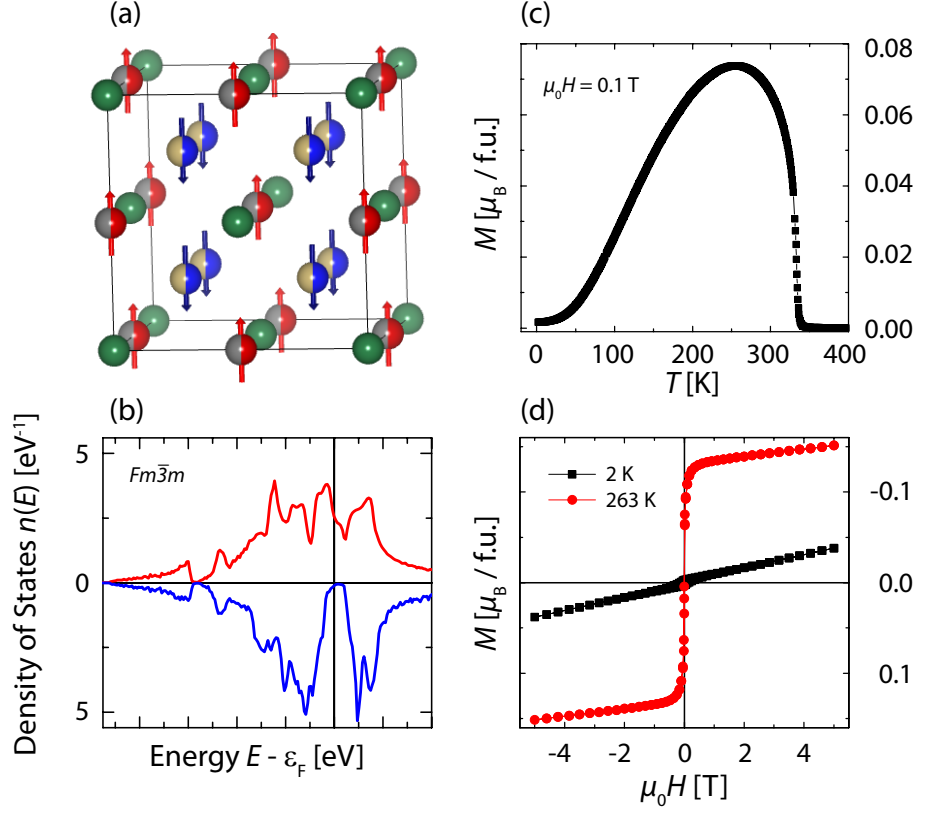


Figure 4

(Color online) (a) Crystal structure of the L21-type cubic Heusler compound $\text{Mn}_{1.5}\text{FeV}_{0.5}\text{Al}$ (space group $Fm\bar{3}m$) and the orientation of the magnetic moments on different sub-lattices. Different atoms are represented by balls with different colors. (b) The spin resolved density of states for $\text{Mn}_{1.5}\text{FeV}_{0.5}\text{Al}$. (c) Temperature dependence of magnetization ($M(T)$) measured in a field of 0.01 T for $\text{Mn}_{1.55}\text{V}_{0.3}\text{Fe}_{1.08}\text{Al}_{0.7}$. (d) Field dependence of magnetization ($M(H)$) measured at 2 K and 263 K for $\text{Mn}_{1.55}\text{V}_{0.3}\text{Fe}_{1.08}\text{Al}_{0.7}$.

moment yields a larger localized moment of about $2.57 \mu_B$ for the Mn atoms that are sitting in the octahedrally coordinated 4b position, as compared with a smaller moment of $1.25 \mu_B$ for the tetrahedrally coordinated Mn atoms that sit in the 8c position. The V and Fe atoms exhibit much smaller moments of only $0.43 \mu_B$ and $0.23 \mu_B$, respectively. In this configuration a total moment of $3 \mu_B$ for Mn at the 4b site and $2.96 \mu_B$ for Mn at the 8c site is calculated. A nearly zero net magnetic moment is expected due to the antiparallel alignment of the moments on the two different sub-lattices. The calculation of the total density of states indicates the presence of a pseudo-gap in one of the spin directions, demonstrating a half-metallic character of $\text{Mn}_{1.5}\text{FeV}_{0.5}\text{Al}$ (Figure 4). The experimental verification of the compensated magnetic structure was obtained from the $M(T)$ measurements shown in Figure 4(c). The $M(T)$ measurement performed in a field of 0.01 T exhibits a Curie temperature (T_C) of about 340 K. As the temperature is reduced the magnetization drops to a nearly zero value at 2 K, indicating the presence of a fully compensated magnetic state near

zero temperature. The $M(H)$ loop measured at 2 K exhibit a linear behavior with a nearly zero spontaneous magnetization. This confirms the completely compensated ferrimagnetic nature of $\text{Mn}_{1.5}\text{FeV}_{0.5}\text{Al}$. The $M(H)$ hysteresis curve measured at 263 K displays a small residual moment of about $0.1 \mu_B$, mostly originating from a small compensation arising from the different temperature dependences of the sub-lattice magnetic moments.

2.4. Spin-gapless Semiconductors

Within the subset of Mn-based Heusler compounds, a particularly interesting material is Mn_2CoAl , which is the first example of a spin-gapless semiconductor (SGS) in the Heusler family of compounds (49). Spin gapless Semiconductors were originally proposed by Wang in 2008 (50) and are formed when a gapless semi-conductor is doped with magnetic ions. The *fcc*-type band structure, that is an inherent feature of Heusler compounds, allows for this peculiar electronic feature. When there are between 18 and 30 valence electrons, several energy windows in the band structure have only weakly dispersed bands. A simplified molecular orbital diagram shows how a sequence of doubly and triply degenerate states are successively filled for 18, 21, 24 and 26 valence electrons. Mn_2CoAl with $N_V = 26$, naturally fulfills this requirement. Özdoğan *et al.*, have studied a set of quaternary LiMgPdSn -type materials, predicting five SGSs: CoFeCrAl , CoMnCrSi , CoFeVSi and FeMnCrSb , whereas FeTiVSi is almost a SGS, as the Fermi energy touches the edges of the conduction and valence bands (51). Synthesized and characterized by Ouardi *et al.*, Mn_2CoAl turned out to show a peculiar electronic structure, that was termed a *spin-gapless semiconducting state* (50, 49), which depicts the band-gap in the minority spin-channel, accompanied by an indirect zero-band-gap in the majority spin-channel. The Curie temperature was found to be $T_C = 720 \text{ K}$, with a magnetic moment of about $2 \mu_B$. The carrier concentration below 300 K is nearly independent of temperature, while the Seebeck coefficient is vanishingly small. SGSs are expected to find applications in spintronic devices, especially semiconductor spintronics as the electronic excitations in the gapless state do not require a threshold energy, but the carriers, whether holes or electrons, remain completely spin-polarized. These materials thus may serve, for example, as spin-injectors.

N_V	Materials				
21	FeVTiSi	CoVScSi	FeCrScSi	FeMnScAl	
26	Mn_2CoAl	CoFeCrAl	CoMnCrSi	CoFeVSi	FeMnCrSb
28	CoFeMnSi				

Table 2 Some exemplary spin-gapless semiconductors, exclusively crystallizing in spacegroup 216.

3. HEUSLER 3.0 – UNIAXIAL HEUSLER COMPOUNDS AND NON-COLLINEAR SPIN STRUCTURES

3.1. Tetragonal Heusler Compounds for Spin-Transfer Torque

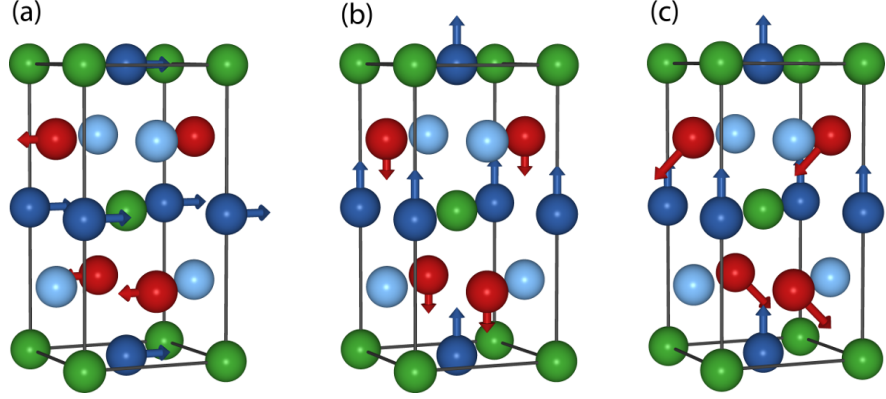


Figure 5

(Color online) A set of generalized tetragonal Heusler structures (spacegroup 119) are shown depicting the four Wyckoff-Positions, that are to be occupied according to Mn (red, blue), Y (light blue), Ga (green, Z) to achieve the *inverse*-type order; (a) In-plane ($K_U < 0$) and (b) out-of-plane ($K_U > 0$) orientation of the magnetization. (c) Exemplary non-collinear order for competing in-plane and out-of-plane anisotropy contributions.

Besides cubic Heusler compounds, which show lots of interesting physics, their structural cousins, the tetragonal Heuslers, are widely studied today. The tetragonal structural modification lowers the symmetry, and unseen effects emerge. Tetragonal Heusler compounds were described by Suits in the 1970s (15, 14), whereas major research began only in the 1990s when research focused on reversible structural phase transitions from cubic to tetragonal lattices, i.e. from austenite to martensite. Shape memory materials rely on this transition, of which Ni_2MnGa (52) and Mn_2NiGa (53) are the flagship materials. The latest boost in tetragonal Heusler compounds research began with the realization that the large magnetocrystalline anisotropy of Mn_3Ga (31, 32) by Balke *et al.*, was of use for spintronic applications. While Co-based materials tend to show soft magnetic properties, the tetragonal distortion induces a preferred orientation of the magnetization towards the in-plane or out-of-plane directions (Figure 5). Perpendicular magnetic anisotropy, with the magnetization pointing perpendicular to the film surface, is desired for high density memory and storage devices to overcome the current limitations, and to guarantee thermal stability. Magnetic memory bits can be switched by either magnetic field or via spin-polarized currents through the concept of spin-transfer-torque. Spin-transfer-torque (STT) refers to a torque that is exerted perpendicular to the magnetization, leading to a precessing magnetic moment, that finally switches to the opposite direction. The Slonczewski-Berger equation (54, 55) describes the dependence of the switching current density on materials properties such as magnetic moment M , anisotropy constant K_U and Gilbert damping parameter α . As the STT technology requires materials with small switching currents while guaranteeing data retention/thermal stability, the Mn-based Heusler compounds have been explored in searches for new tetragonal phases. That said, Alijani *et al.* (56) have studied

the Mn-Co-Ga system (57), testing the stability of the tetragonal Mn_3Ga phase with the substitution of Mn by Co: $\text{Mn}_{3-x}\text{Co}_x\text{Ga}$. A tetragonal phase is maintained until a critical Co concentration of $x_{\text{Co}} = 0.5$. The subsequent members with higher Co concentration exhibited the inverted cubic structure with mixed Mn-Co sites. In agreement with a subsequent theoretical treatment, the magnetic moments of the tetragonal phases decrease with increasing cobalt content. Surprisingly, an approximately linear relationship between the number of valence electrons and the magnetic moment was found for these and other tetragonal Heusler phases (40), such as Mn_2CrGa , Mn_3Ga , Mn_2FeGa , Mn_2CoGa . These phases were modeled by density functional theory and a local energy minimum in the energy landscape could be observed. Nevertheless, the tetragonal phase does not show half-metallic behavior, which renders this observation particularly surprising. But this theoretical study provided evidence for the correlation of the tetragonal distortion with the peak and valley structure of the density of states. For the case that the Fermi edge resides at a peak in the DOS, a distorted structure is likely to occur (Mn-Ga, Mn-Ni-Ga, Mn-Fe-Ga) as a slight distortion breaks either the bands' degeneracy or changes the band dispersion such that the electronic susceptibility is diminished. Mn_2CoGa is found to be cubic as the Fermi edge is located at a local minimum in the DOS of both spin-channels. Studying the transport properties of the Mn-Co-Ga series revealed another effect that is termed *spin-selective electron localization* (58, 59). Spin-selective electron localization describes the change in conductivity polarization for transition metal substituted Mn_3Ga -systems. The exchange of Mn with a transition metal ($Y = \text{Sc}, \text{Ti}, \text{V}, \text{Cr}, \text{Fe}, \text{Co}, \text{Ni}$) leads to an increase in spin-polarization since only one spin-channel is perturbed by the substitution.

3.2. Tetragonal Compensated Ferrimagnetic Heusler Compounds

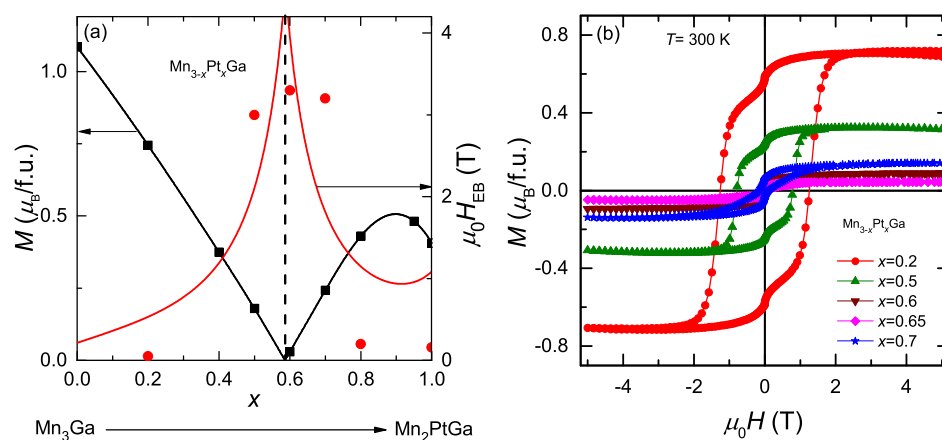


Figure 6

(Color online) (a) Theoretical calculation of magnetic moment (solid squares, left axis) as a function of Pt content in $\text{Mn}_{3-x}\text{Pt}_x\text{Ga}$. The line connecting the solid squares is a guide to the eye. Exchange bias field (H_{EB}) as a function of Pt concentration x_{Pt} (right axis). Solid circles show the experimental data, whereas, the solid curve corresponds to a model calculation. (b) Curves for $\text{Mn}_{3-x}\text{Pt}_x\text{Ga}$ thin films measured at 300 K.

Tetragonal magnetic materials with out of plane magnetic anisotropy are of great interest for spin transfer torque (STT) and permanent magnet related applications. It is well known that the Mn-based tetragonal Heuslers are ferrimagnetic in nature with at least two magnetic sub-lattices, where the magnetic moments align antiparallel to each other (32, 33, 60, 61, 62, 63, 64, 39, 40, 65). In addition, they exhibit high magnetic ordering temperatures well above room temperature, which is a necessary condition for any practical application. The best example of a tetragonal magnetic Heusler is Mn_3Ga which shows a ferrimagnetic ordering with T_C of about 750 K (32). Despite these ideal characteristics, ferro/ferri magnets exhibit large unwanted stray fields that affect the magnetic state of neighboring layers in multilayer spintronic devices or neighboring devices in arrays of devices. We have proposed that a fully compensated ferrimagnetic state with a zero net magnetic moment can be achieved by systematically tuning the sub-lattice magnetic moments in Mn_3Ga (66). From theoretical calculations we have shown that the compensated magnetic state can be achieved for a wide range of Heusler materials by substituting a late transition metal element in $\text{Mn}_{3-x}\text{Y}_x\text{Ga}$ including Ni, Cu, Rh, Pd, Ag, Ir, Pt and Au (67).

A specific example of magnetic compensation when $Y = \text{Pt}$ is shown in Figure 6(a). Mn_3Ga consists of two non-equivalent types of Mn atoms, one within the Mn-Ga and one within the Mn-Mn planes of the tetragonal structure with space group $I4/mmm$. The Mn sitting in the Mn-Ga planes possess a larger localized moment of about $3.1 \mu_B$ compared to a moment of $2.1 \mu_B$ for the Mn sitting in the Mn-Mn plane. However, a larger total moment of $4.2 \mu_B/\text{f.u.}$ is expected from the Mn sitting in the Mn-Mn plane as there are two Mn/f.u. (formula unit) in this plane. One way of reducing the magnetic moments of the Mn sitting in the Mn-Mn plane to match that of the moment of the single Mn in the Mn-Ga plane is by partially substituting Mn in the Mn-Mn plane by a non-magnetic element. We have shown that for a Pt concentration of approximately $x = 0.6$ in $\text{Mn}_{3-x}\text{Pt}_x\text{Ga}$, the Mn atoms in the Mn-Mn(Pt) and the Mn atom in the Mn-Ga planes contribute nearly the same moment with opposite alignment. As demonstrated in Figure 6(a), with increasing Pt concentration, the total magnetic moment decreases and becomes zero at $x = 0.6$ before further increasing for higher Pt concentrations. The theoretical concept is nicely verified by growing thin films with different Pt concentrations. As shown in Figure 6(b), $M(H)$ loops measured at 300 K for different thin films exhibit typical out of plane hysteretic behavior found in a tetragonal system. The sample with a Pt concentration $x = 0.2$, exhibits a magnetic moment of $0.7 \mu_B/\text{f.u.}$ at 300 K. The magnetization starts decreasing with increasing Pt content and becomes nearly zero for $x = 0.65$, demonstrating a fully compensated ferrimagnetic state for $\text{Mn}_{2.35}\text{Pt}_{0.65}\text{Ga}$. As expected, the magnetization starts increasing again for further increases in the Pt concentration. Most importantly, these thin films show magnetic ordering temperatures well above room temperature. The feasibility of the practical application of these tetragonally compensated ferrimagnets has been demonstrated by showing the existence of a large exchange bias both in bulk and bilayer thin film materials (68, 66, 67).

3.3. Non-collinear magnetic structure

There has been much recent interest in magnetic materials exhibiting non-collinear spin structures. One of the most exciting uses of non-collinear spin structure is the motion of chiral domain walls using spin polarized currents that generate a large chiral spin-orbit torques to drive the domain walls (69, 70). This current driven back and forth motion of the domain walls inside a magnetic nano-wire forms a novel high density, high perfor-

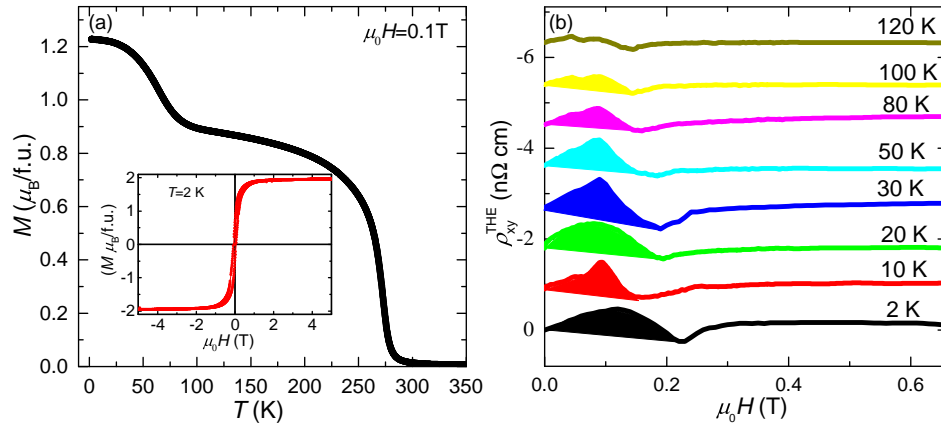


Figure 7

(Color online) (a) $M(T)$ curve measured in a field of 0.1 T for the Heusler tetragonal compound Mn_2RhSn . The inset shows $M(H)$ loop measured at 2 K. (b) Topological Hall effect (ρ_{xy}^T) at different temperatures for the Mn_2RhSn thin film.

mance, solid-state storage memory device - Racetrack Memory - that was first proposed by Parkin *et al.* in 2002 and which has the potential to even replace conventional magnetic data storage (71). The domain wall can be replaced by other non-collinear spin textures such as skyrmions (72). In this regard, Heusler materials are perfect candidates to modify the magnetic state via competing exchange interactions between different sub-lattices (66). In addition, most of the Mn-based Heusler materials exhibit a non-centrosymmetric crystal structure, which is necessary for the realization of the Dzyaloshinskii-Moriya (DM) interaction that leads to the formation of skyrmions (73).

The direct evidence of non-collinear magnetic state was found in the non-centrosymmetric tetragonal Heusler compound Mn_2RhSn (73). As shown in Figure 7(a), Mn_2RhSn exhibits a T_C of about 275 K with a transition to a state with a comparatively higher magnetic moment at about 80 K. The magnetic ordering at the low temperature has been assigned to a spin-reorientation transition. The $M(H)$ loop measured at 2 K shows a saturation magnetization of about $2 \mu_B$ (inset of Figure 7), which cannot be accounted for by considering a collinear spin arrangement. In Mn_2RhSn , Mn atoms occupy two distinct sub-lattices. The Mn sitting in the Mn-Sn planes (MnI) show a moment of nearly $3.6 \mu_B$, whereas, the Mn in the Mn-Rh planes (MnII) exhibits a moment of about $3 \mu_B$. A simple antiparallel alignment between the moments of MnI and MnII will give a net moment of $0.6 \mu_B$. However, this simplified model does not match the experimentally determined magnetic moment of $2 \mu_B$. Similarly, a ferromagnetic ordering will result in a total moment of $6.6 \mu_B$, that also does not fit to the observed moment. However, the experimental magnetic moment can be explained nicely by considering a non-collinear magnetic structure in Mn_2RhSn . The theoretical calculations show that the competition between the antiferromagnetic interaction between the Mn moments in nearest and next-nearest planes can give rise to a canting of the MnII moment of about 55° , thereby, providing an additional z-component of the moment to the simple ferrimagnetic configuration. The theoretical results are supported by evidence of a non-collinear spin configuration from neutron diffraction measurements (73).

Theoretical calculations also show that the present class of materials with accentric crystal structures should give rise to the formation of skyrmions under appropriate conditions. However, the experimental finding of skyrmions in bulk materials is still awaited. Recently, it has been shown that the thin films of Mn_2RhSn exhibit a considerable topological Hall effect (THE) as shown in Figure 7(b). The THE was obtained in temperatures of up to 100 K, which is the spin-reorientation transition in thin film samples. Note that materials that have skyrmions also exhibit a large THE due to their chiral non-collinear spin structures (74, 75). Hence, it can be assumed that there is some type of non-collinear spin structure like skyrmions present in Mn_2RhSn (76).

4. HEUSLER 4.0 – TOPOLOGICAL HEUSLER COMPOUNDS

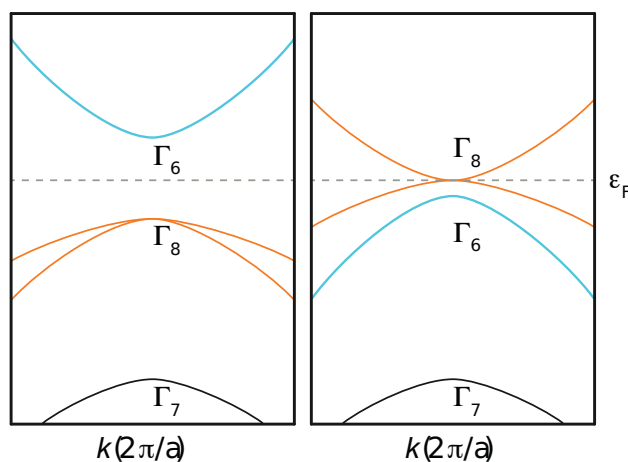


Figure 8

(Color online) Schematic of a trivial and inverted band structure as found in (a) CdTe and (b) HgTe

The prediction of the Quantum Spin Hall (QSH) state (77) triggered tremendous interest in the condensed matter community. It not only lay the foundation for a completely new field of research, but the use and application of topological concepts in a wide range of condensed matter research gained much attention. The QSH state was subsequently realized in a HgTe/CdTe quantum well structure (78): materials that crystallize in the same space group ($F43m$) as the XZ binary semiconductors (HgTe, CdTe, ZnS) include diamond and the *Half*-Heusler compounds. *Half*-Heusler semiconductors with 8 or 18 VEs exist with a wide range of band-gaps (79, 80), and the possibility to find *half*-Heuslers with a topologically non-trivial state was quickly realized (81, 82). A set of *half*-Heuslers that could be classified into topologically trivial and potentially non-trivial materials was proposed. Non-trivial HgTe exhibits a band-inversion of the Γ_6 and Γ_8 states at the Γ point. Chadov *et al.* could show that zero-gap semiconductors within the *half*-Heusler family exhibit similar features, and an odd number of band inversions is observed in some systems. The flexibility of the Heusler compounds with respect to site occupation provides the means of tuning these materials from trivial to non-trivial states by means of lattice parameter adjustment through substitution of isoelectronic elements or adequate hybridization strength. Since the band inversion results from spin-orbit coupling, another recipe is by strengthening of the average spin-orbit interaction via, for example, substitution by heavy transition metals. Some of the zero-gap semiconductors that have been experimentally realized show a surprising range of multifunctional properties in addition to the non-trivial electronic structure, when rare earth elements are introduced, as for example: GdPtBi – antiferromagnetism (83), LaPtBi – superconductivity ($T_{\text{crit.}} < 0.9 \text{ K}$) (84), YPtBi – heavy fermion behavior and superconductivity ($T_{\text{crit.}} < 0.9 \text{ K}$) (85, 86), ErPtBi – antiferromagnetism ($T_N < 1.2 \text{ K}$) (83). The zero-gap state, that is a prerequisite for topological insulators, is also a useful feature for thermoelectric materials. Consequently, a connection between topological insulators, the zero-gap-state, and thermoelectric performance is profound (87).

4.1. GdPtBi – a Weyl-Semimetal in a magnetic field

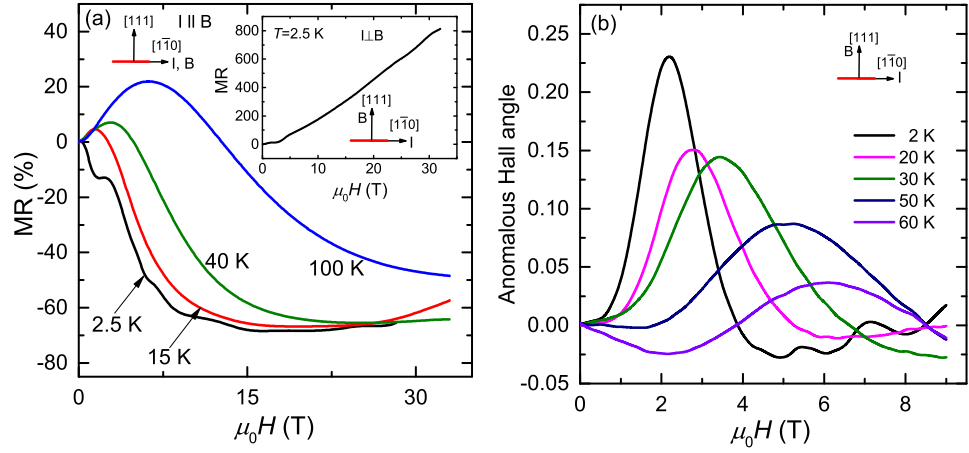


Figure 9

(Color online) (a) Field dependence of longitudinal magnetoresistance (MR) measured at different temperatures for fields up to 33 T in GdPtBi for the crystal directions shown in the figure. The inset shows the transverse MR measured at 2.5 K. (b) Anomalous Hall angle (AHA) at different temperatures for GdPtBi.

Weyl semimetals (WSM) are a class of topological semimetals, beyond topological insulators, where the conduction and valence bands cross in the vicinity of the Fermi level (88, 89, 90, 91, 92, 93, 94, 95, 96, 97, 98, 99, 100). The crossing points are called Weyl points that are separated in momentum space. These Weyl points, which act as magnetic monopoles in momentum space, always appear in pairs and are connected by an unusual surface state termed the Fermi arc (97, 98, 101, 102, 103, 99). In general, semimetals exhibit ultra-high carrier mobilities and large transverse magnetoresistance values (MR), that are also promising effects for spintronic applications (104, 105, 106). However, the non-trivial electronic structure of a WSM can give rise to additional unusual phenomena such as negative magnetoresistance which is connected to chiral magnetic effects (90, 96). The chiral anomaly comes from the charge pumping between two Weyl points connected through the Fermi arc. In most of the three dimensional WSMs, where the breaking of either time reversal symmetry or inversion symmetry occurs, the Weyl points come as a result of accidental touching/crossing of the conduction and valence bands. In recent work, however, experimental evidence of an unusual topological surface state (107) and a chiral anomaly (108) have been found in the lanthanide *half*-Heusler semimetals.

The existence of negative MR that is associated with a chiral anomaly in these lanthanide *half*-Heuslers was attributed to the formation of Weyl points due to an external field induced Zeeman splitting. However, it is presumed that the Zeeman splitting is negligible in comparison to the much larger exchange-field coming from the 4f electrons in *RE*PtBi compounds (*RE* = Gd, Nd). Both GdPtBi and NdPtBi are antiferromagnetic below their respective Néel temperatures of 9.0 K and 2.1 K (109, 110, 111). In the absence of an external field, the exchange fields originating from the magnetic moments at different sub-lattices cancel and, hence, no Weyl points are observed. With the application of a modest external

magnetic field the Gd moments in different sub-lattices align parallel to each other resulting in a ferromagnetic ordering. Thus, the exchange-splitting of the conduction bands can give rise to the formation of Weyl points.

The existence of a large unsaturated longitudinal negative MR in GdPtBi is shown in Figure 9(a). The MR measurements have been performed up to fields of 33 T with I parallel to B with the configuration shown in the figure. A large negative MR of 68% is observed at 2.5 K. The negative MR persists up to temperatures greater than 100 K, which is much above the T_N of GdPtBi (112). However, the field required to give a negative MR increases with increasing temperature due to thermal effects. As shown in the inset of Figure 9(a), a large transverse positive MR is observed when the magnetic field is applied perpendicular to the current. These experiments confirm that the negative MR in GdPtBi originates from the formation of Weyl points due to the field driven splitting of the conduction band. Another proof of the chiral anomaly is the finding of a large anomalous Hall effect in GdPtBi. A large anomalous Hall angle (AHA) of about 0.23 is calculated in a field of 2.2 T at 2 K. The AHA decreases with increasing temperature and the field where a maximum AHE is observed shifts to higher magnetic fields. This indicates that the AHE is closely related to the presence of negative MR originating from the chiral anomaly.

4.2. Co₂TiSn – a magnetic, centrosymmetric Weyl semimetal

Crossing points in the electronic band structure, such as Weyl and Dirac points, are not rare, but very often these points are not at the Fermi energy or many other bands also cross the Fermi energy. Weyl and Dirac points have a strong influence on the transport properties and other properties if they are very close to the Fermi energy in a semimetal. It is established and nicely described in the review of Nagaosa *et al.* (113) that these crossing points in the electronic structure lead to an enhanced Berry phase and, therefore, to a large anomalous Hall effect (AHE) in magnetic systems and to a spin Hall effect (SHE) in paramagnetic metals or diamagnetic topological semimetals. It is reported that these points act as a magnetic monopole for the Berry curvature in momentum space (114). A large AHE in connection with a large Berry phase in Heusler compounds was predicted by Kübler and Felser for Co₂MnAl (115). The predicted value of the giant AHE was in excellent agreement with the experimentally determined value (116). Husmann *et al.* (117) investigated Co₂CrAl and found that the intrinsic AHE dominates. An intrinsic contribution comes from the Berry phase while extrinsic contributions originate from scattering from impurities through skew scattering and side jump contributions. It is noteworthy that Kübler and Felser had already noted a Dirac point below the Fermi energy in Co₂VSn, but a direct connection between the giant AHC and the Dirac point was not made (115). In the context of recent searches for Weyl and Dirac points in the electronic structure of semimetals Wang *et al.* (118) and Chang *et al.* (119) proposed that electron doped Co₂TiSn should be a magnetic Weyl semimetal. Based on the work on AHE, Kübler and Felser recognized that Co₂MnAl is a Weyl metal even when undoped. It seems that there is a relation between the Weyl semimetals and the spin gapless semimetals. SGSs appear only in the non-centrosymmetric space group 216 ($F\bar{4}3m$), whereas for the same number of valence electrons the corresponding Heusler compounds in space group 225 ($Fm\bar{3}m$) are Weyl semimetals. The minority band structures for the respective materials are identical in both space groups, but the bands are not allowed to cross in the space group 225 and turn to a forbidden crossing and therefore a semiconducting majority spin-channel is obtained instead

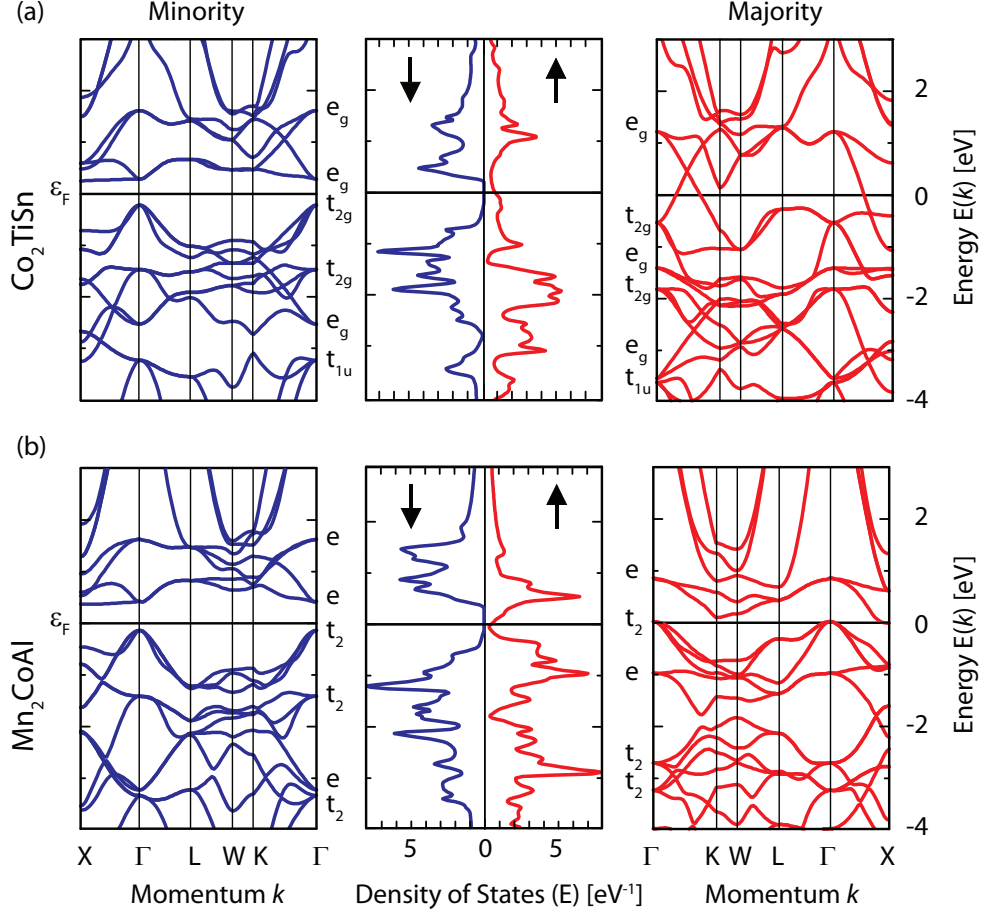


Figure 10

(Color online) Spin resolved band structure and density of states of (a) the magnetic Weyl semimetal Co_2TiSn and (b) the spin-gapless semiconductor Mn_2CoAl , both with 26 valence electrons.

of a Weyl semimetal (See Figure 10). This concept can help to identify Weyl semiconductors and non centro-symmetric semiconductors via simple electron counting rules.

4.2.1. Topological non-cubic Heuslers. The existence of a non-collinear magnetic structure in tetragonal Heusler materials is discussed in the previous section (73, 76). Many of these Mn-based Heusler materials also exhibit a stable hexagonal crystal structure (120, 121, 122, 123). By varying the preparation conditions cubic, tetragonal and hexagonal phase can be stabilized in one system (124). It turns out that most of the hexagonal materials display an antiferromagnetic ordering (120). Neutron diffraction studies of the hexagonal Mn_3Sn and Mn_3Ge compounds reveal the presence of a non-collinear antiferromagnetic ordering (122). In particular, hexagonal Mn_3Ge , which consists of two layers of Mn triangles stacked along the c -axis, shows a 120° -triangular antiferromagnetic structure (122). As

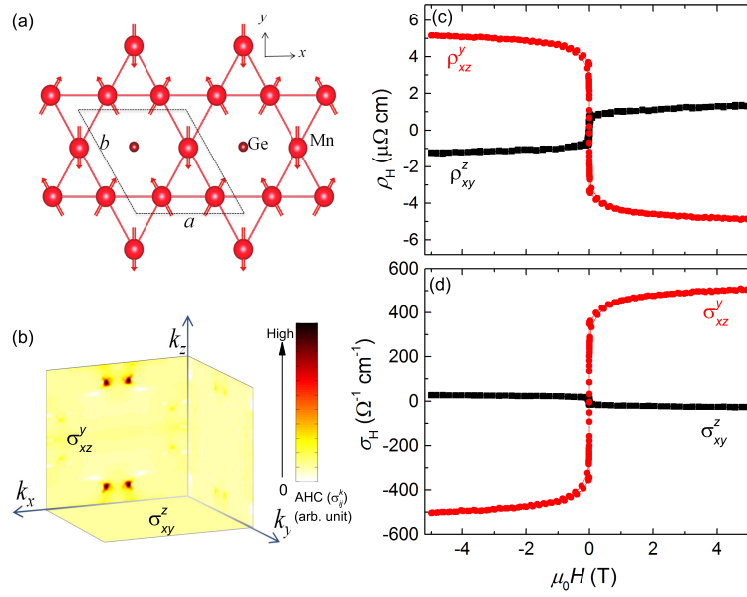


Figure 11

(Color online) (a) Triangular non-collinear antiferromagnetic configuration for hexagonal Mn₃Ge. (b) Berry curvature integrated along the k_x , k_y and k_z axes, plotted in the $k_y k_z$, $k_x k_z$ and $k_x k_y$ planes, respectively. For the spin configuration shown in a, only a nonzero anomalous Hall conductivity (σ_{xz}^y) is obtained in the $k_x - k_z$ plane. (c) Hall resistivity (ρ_H) as a function of magnetic field (H) measured at 2 K. (d) Field dependence of Hall conductivity (σ_H) obtained from the corresponding Hall resistivities shown in (c).

shown in Figure 11 (a), the Mn atoms form a Kagome lattice with Ge sitting at the center of a hexagon. The non-collinear spin structure arises due from geometrical frustration of the Mn spins arranged in the triangular spin structure. Recent theoretical works have demonstrated that materials with non-collinear antiferromagnetic structures and with some special symmetries should exhibit a large anomalous Hall effect (AHE) (125, 126). Note that the AHE is an intrinsic property of all ferromagnets and roughly scales with the magnetization (113). Therefore, antiferromagnets with a zero net magnetic moment, in general, should not display an AHE. Since the intrinsic AHE is a manifestation of the Berry curvature, we have calculated the Berry curvature in Mn₃Ge by considering the non-collinear antiferromagnetic spin structure shown in Figure 11 (a). The distribution of Berry curvature in the momentum space is depicted in Figure 11 (b). It can be clearly seen that a non-vanishing Berry curvature is only obtained in the $k_x - k_z$ plane, and almost zero amplitudes of the Berry curvature are observed in other two planes. (127) Our theoretical predictions were supported by measuring the experimental AHE in Mn₃Ge, as shown in Figure 11 (c) and (d). A large anomalous Hall resistivity (ρ_H) of $5.1 \mu\Omega$ cm was found in the $x - z$ plane (ρ_{xz}^y), whereas, a small (ρ_H) of about $5.1 \mu\Omega$ was measured in the $x - y$ plane (ρ_{xy}^z). Similarly, an extremely large AHC of about $500 \Omega \text{cm}^{-1}$ and almost zero AHC are calculated in the $x - z$ (σ_{xz}^y) and $x - y$ (σ_{xy}^z) planes, respectively (127). A similarly large AHE has been also been found in the hexagonal non-collinear antiferromagnetic Mn₃Sn (128). It

is worth noting that the ferromagnetic Heusler compounds Co_2MnSi and Co_2MnGe with a net magnetic moment of about $5 \mu_{\text{B}}$ display a maximum ρ_{H} of $4 \mu\Omega$ (129). Thus, the finding of such a large AHE in the antiferromagnetic Mn_3Ge and Mn_3Sn can be explored further for their possible use in antiferromagnetic spintronics (130).

5. SUMMARY

The Heusler compounds have a rich history dating back more than a century and yet fascinating new properties continue to emerge even today. In this review we have elaborated the history of Heuslers in 4 distinct development phases. In Heusler 1.0 the discovery of combinations of essentially non-magnetic elements that form ferromagnetic compounds well above room temperature was a remarkable finding. In Heusler 2.0 the theoretical prediction and experimental finding of half-metallicity in certain classes of Heusler materials was another major discovery that would lead several decades later to the funding of giant value of tunneling magnetoresistance. In Heusler 4.0 more complex magnetic structures in which the magnetic moments are aligned non-collinearly have been discovered in a range of Heusler compounds. In Heusler 3.0 an entirely new world of Heusler compounds was revealed by the application of newly developed notions of topology that led to the prediction and later experimental proof of topological insulators and, more recently, Weyl semi-metallic Heuslers. What is perhaps even more remarkable is that many of these properties evolve from simple concepts of electron counting. By changing the number of valence electrons the magnetization and Curie temperature of magnetic Heuslers can be varied systematically or the Weyl points in their band structure can be tuned though the Fermi energy. In this review there was no space to describe other properties of the Heuslers that include, for example, giant thermoelectricity or the magnetocaloric applications. Heusler compounds are promising for a wide range of applications that has focussed to date on spintronic applications. The future for Heuslers seems very bright.

DISCLOSURE STATEMENT

The authors are not aware of any affiliations, memberships, funding, or financial holdings that might be perceived as affecting the objectivity of this review.

ACKNOWLEDGMENTS

Financial support from the *European Research Council Advanced Grant* (ERC-AG; No. 291472 “IDEA Heusler!”) is gratefully acknowledged.

LITERATURE CITED

1. Heusler F. 1903. Ueber magnetische Manganlegierungen. *Verh. Dtsch. Phys. Ges.* 5:219
2. Heusler F, W. S, Haupt E. 1903. Magnetisch-Chemische Studien. *Verh. Dtsch. Phys. Ges.* 5:220
3. Néel L. 1936. Propriétés magnétiques de l'état magnétique et énergie d'interaction entre atomes magnétiques. *Ann. de Phys.* 5:232–279

4. Néel L. 1953. Some new results on antiferromagnetism and ferromagnetism. *Rev. Mod. Phys.* 25:58–63
5. Heusler O. 1934. Kristallstruktur und Ferromagnetismus der Mangan-Aluminium-Kupferlegierungen. *Adv. Phys.* 411:155–201
6. Bradley AJ, Rodgers JW. 1934. The crystal structure of the Heusler alloys. *Proc. Roy. Soc. (London) A* 144:340–359
7. Castelliz L. 1951. Eine ferromagnetische Phase im System Nickel-Mangan-Antimon. *Monatsh. Chem.* 82:1059–1085
8. Castelliz L. 1952. Über eine Mischkristallreihe zwischen zwei terären Vertretern des C1-Typs. *Monatsh. Chem.* 83:1314–1317
9. Graf T, Felser C, Parkin SSP. 2011. Simple rules for the understanding of Heusler compounds. *Prog. Solid State Ch.* 39:1–50
10. Webster P. 1971. Magnetic and chemical order in Heusler alloys containing cobalt and manganese. *J. Phys. Chem. Solids* 32:1221 – 1231
11. Webster PJ, Tebble RS. 1967. The magnetic and chemical ordering of the Heusler alloys Pd_2MnIn , Pd_2MnSn and Pd_2MnSb . *Phil. Mag.* 16:347–361
12. Morris DP, Preston RR, Williams I. 1959. Search for new Heusler alloys. *Proc. Phys. Soc.* 73:520
13. Webster P, Ramadan M. 1977. Magnetic order in palladium-based Heusler alloys part i: $\text{Pd}_2\text{MnIn}_{1-x}\text{Sn}_x$ and $\text{Pd}_2\text{MnSn}_{1-x}\text{Sb}_x$. *J. Magn. Magn. Mater.* 5:51 – 59
14. Suits J. 1976. Structural instability in new magnetic Heusler compounds. *Solid State Commun.* 18:423 – 425
15. Suits JC. 1976. New magnetic compounds with Heusler and Heusler-related structures. *Phys. Rev. B* 14:4131–4135
16. Felser C, Fecher G, Balke B. 2007. Spintronics: A challenge for materials science and solid-state chemistry. *Angewandte Chemie International Edition* 46:668–699
17. de Groot RA, Mueller FM, van Engen PG, Buschow KHJ. 1983. New class of materials: Half-metallic ferromagnets. *Phys. Rev. Lett.* 50:2024–2027
18. Ishida S, Akazawa S, Kubo Y, Ishida J. 1982. Band theory of Co_2MnSn , Co_2TiSn and Co_2TiAl . *J. Phys. F: Met. Phys.* 12:1111
19. Vosko SH, Wilk L, Nusair M. 1980. Accurate spin-dependent electron liquid correlation energies for local spin density calculations: a critical analysis. *Can. J. Phys.* 58:1200–1211
20. Kübler J, William AR, Sommers CB. 1983. Formation and coupling of magnetic moments in Heusler alloys. *Phys. Rev. B* 28:1745
21. Friedel J. 1958. Metallic alloys. *Il Nuovo Cim.* 7:287–311
22. Fecher GH, Kandpal HC, Wurmehl S, Felser C, Schnhense G. 2006. Slater-pauling rule and curie temperature of Co_2 -based heusler compounds. *J. Appl. Phys.* 99
23. Skaftouros S, Özdoğan K, Şaşıoğlu E, Galanakis I. 2013. Generalized Slater-Pauling rule for the *inverse* Heusler compounds. *Phys. Rev. B* 87:024420
24. Ouardi S, Fecher GH, Balke B, Beleanu A, Kozina X, et al. 2011. Electronic and crystallographic structure, hard x-ray photoemission, and mechanical and transport properties of the half-metallic Heusler compound Co_2MnGe . *Phys. Rev. B* 84:155122
25. Kübler J, Fecher GH, Felser C. 2007. Understanding the trend in the Curie temperatures of Co_2 -based Heusler compounds: *Ab initio* calculations. *Phys. Rev. B* 76:024414
26. Kübler J. 2000. Theory of itinerant electron magnetism. Oxford Univ. Press
27. Block T, Felser C, Jakob G, Ensling J, Mühling B, et al. 2003. Large negative magnetoresistance effects in $\text{Co}_2\text{Cr}_{0.6}\text{Fe}_{0.4}\text{Al}$. *J. Solid State Chem.* 176:646–651
28. Liu Hx, Honda Y, Taira T, Matsuda Ki, Arita M, et al. 2012. Giant tunneling magnetoresistance in epitaxial $\text{Co}_2\text{MnSi}/\text{MgO}/\text{Co}_2\text{MnSi}$ magnetic tunnel junctions by half-metallicity of Co_2MnSi and coherent tunneling. *Appl. Phys. Lett.* 101
29. Jourdan M, Minár J, Braun J, Kronenberg A, Chadov S, et al. 2014. Direct observation of

- half-metallicity in the Heusler compound Co_2MnSi . *Nat. Commun.* 5
30. Weht R, Pickett WE. 1999. Half-metallic ferrimagnetism in Mn_2VAl . *Phys. Rev. B* 60:13006–13010
 31. Krén E, Kádár G. 1970. Neutron diffraction study of Mn_3Ga . *Solid State Commun.* 8:1653–1655
 32. Balke B, Fecher GH, Winterlik J, Felser C. 2007. Mn_3Ga , a compensated ferrimagnet with high Curie temperature and low magnetic moment for spin torque transfer applications. *Appl. Phys. Lett.* 90:152504
 33. Winterlik J, Balke B, Fecher GH, Felser C, Alves MCM, et al. 2008. Structural, electronic, and magnetic properties of tetragonal Mn_{3-x}Ga : Experiments and first-principles calculations. *Phys. Rev. B* 77:054406
 34. Kopp WU, Wachtel E. 1969. Magnetic properties of solid and liquid Al-Mn alloys containing Cr, V or Ti. *Z. Metallkd.* 60:713
 35. Nakamichi T, Itoh H. 1978. Magnetic properties of Mn-V-Al ternary alloys. *Z. Metallkd.* 69:344–350
 36. Itoh H, Nakamichi T, Yamaguchi Y, Kazama N. 1983. Neutron diffraction study of Heusler type alloy $\text{Mn}_{0.47}\text{V}_{0.28}\text{Al}_{0.25}$. *T. Jpn. I. Met.* 24:265–271
 37. Galanakis I, Dederichs PH, Papanikolaou N. 2002. Origin and properties of the gap in the half-ferromagnetic Heusler alloys. *Phys. Rev. B* 66:134428
 38. Özdoğan K, Galanakis I, Şaşıoğlu E, Aktaş B. 2006. Search for half-metallic ferrimagnetism in V-based Heusler alloys Mn_2VZ ($Z = \text{Al, Ga, In, Si, Ge, Sn}$). *J. Phys.: Condens. Matter* 18:2905–2914
 39. Wollmann L, Chadov S, Kübler J, Felser C. 2014. Magnetism in cubic manganese-rich Heusler compounds. *Phys. Rev. B* 90:214420
 40. Wollmann L, Chadov S, Kübler J, Felser C. 2015. Magnetism in tetragonal manganese-rich Heusler compounds. *Phys. Rev. B* 92:064417
 41. Wurmehl S, Kandpal HC, Fecher GH, Felser C. 2006. Valence electron rules for prediction of half-metallic compensated-ferrimagnetic behaviour of Heusler compounds with complete spin polarization. *J. Phys.: Condens. Matter* 18:6171–6181
 42. Burch TJ, Litrenta T, Budnick JI. 1974. Hyperfine studies of site occupation in ternary systems. *Phys. Rev. Lett.* 33:421–424
 43. Luo H, Zhu Z, Ma L, Xu S, Zhu X, et al. 2008. Effect of site preference of 3d atoms on the electronic structure and half-metallicity of Heusler alloy Mn_2YAl . *J. Phys. D: Appl. Phys.* 41:055010
 44. Slater JC. 1936. The ferromagnetism of nickel. ii. temperature effects. *Phys. Rev.* 49:931–937
 45. Pauling L. 1938. The nature of the interatomic forces in metals. *Phys. Rev.* 54:899–904
 46. Kurt H, Rode K, Stamenov P, Venkatesan M, Lau YC, et al. 2014. Cubic Mn_2Ga thin films: Crossing the spin gap with ruthenium. *Phys. Rev. Lett.* 112:027201
 47. Betto D, Thiyagarajah N, Lau YC, Piamonteze C, Arrio MA, et al. 2015. Site-specific magnetism of half-metallic $\text{Mn}_2\text{Ru}_x\text{Ga}$ thin films determined by x-ray absorption spectroscopy. *Phys. Rev. B* 91:094410
 48. Stinshoff R, Fecher GH, Felser C. 2016. Completely compensated half-metallic ferrimagnetism and sublattice spin crossing in the Heusler compound $\text{Mn}_{1.5}\text{FeV}_{0.5}\text{Al}$. *Phys. Rev. B* submitted
 49. Ouardi S, Fecher GH, Felser C, Kübler J. 2013. Realization of spin gapless semiconductors: The Heusler compound Mn_2CoAl . *Phys. Rev. Lett.* 110:100401
 50. Wang XL. 2008. Proposal for a new class of materials: Spin gapless semiconductors. *Phys. Rev. Lett.* 100:156404
 51. Özdoğan K, Şaşıoğlu E, Galanakis I. 2013. Slater-Pauling behavior in LiMgPdSn -type multifunctional quaternary Heusler materials: Half-metallicity, spin-gapless and magnetic semiconductors. *J. Appl. Phys.* 113
 52. Ullakko K, Huang JK, Kantner C, O’Handley RC, Kokorin VV. 1996. Large magnetic field in-

- duced strains in Ni_2MnGa single crystals. *Appl. Phys. Lett.* 69:1966–1968
53. Liu GD, Dai XF, Yu SY, Zhu ZY, Chen JL, et al. 2006. Physical and electronic structure and magnetism of Mn_2NiGa : Experiment and density-functional theory calculations. *Phys. Rev. B* 74:054435
 54. Slonczewski J. 1996. Current-driven excitation of magnetic multilayers. *J. Magn. Magn. Mater.* 159:L1 – L7
 55. Berger L. 1996. Emission of spin waves by a magnetic multilayer traversed by a current. *Phys. Rev. B* 54:9353–9358
 56. Alijani V, Winterlik J, Fecher GH, Felser C. 2011. Tuning the magnetism of the Heusler alloys $\text{Mn}_{3-x}\text{Co}_x\text{Ga}$ from soft and half-metallic to hard-magnetic for spin-transfer torque applications. *Appl. Phys. Lett.* 99:222510
 57. Ouardi S, Kubota T, Fecher GH, Stinshoff R, Mizukami S, et al. 2012. Stoichiometry dependent phase transition in Mn-Co-Ga-based thin films: From cubic in-plane, soft magnetized to tetragonal perpendicular, hard magnetized. *Appl. Phys. Lett.* 101:242406
 58. Wollmann L, Fecher GH, Chadov S, Felser C. 2015. A scheme for spin-selective electron localization in Mn_3Ga Heusler material. *J. Phys. D: Appl. Phys.* 48:164004
 59. Chadov S, D'Souza SW, Wollmann L, Kiss J, Fecher GH, Felser C. 2015. Chemical disorder as an engineering tool for spin polarization in Mn_3Ga -based Heusler systems. *Phys. Rev. B* 91:094203
 60. Winterlik J, Fecher GH, Balke B, Graf T, Alijani V, et al. 2011. Electronic, magnetic, and structural properties of the ferrimagnet Mn_2CoSn . *Phys. Rev. B* 83:174448
 61. Klaer P, Jenkins CA, Alijani V, Winterlik J, Balke B, et al. 2011. Disentangling the mn moments on different sublattices in the half-metallic ferrimagnet $\text{Mn}_{3-x}\text{Co}_x\text{Ga}$. *Appl. Phys. Lett.* 98:212510
 62. Nayak AK, Shekhar C, Winterlik J, Gupta A, Felser C. 2012. Mn_2PtIn : A tetragonal Heusler compound with exchange bias behavior. *Appl. Phys. Lett.* 100:152404
 63. Gasi T, Nayak AK, Winterlik J, Ksenofontov V, Adler P, et al. 2013. Exchange-spring like magnetic behavior of the tetragonal Heusler compound Mn_2FeGa as a candidate for spin-transfer torque. *Appl. Phys. Lett.* 102:202402
 64. Kurt H, Baadji N, Rode K, Venkatesan M, Stamenov P, et al. 2012. Magnetic and electronic properties of $\text{D}_{022}\text{-Mn}_3\text{Ge}$ (001) films. *Appl. Phys. Lett.* 101:132410
 65. Jeong J, Ferrante Y, Faleev SV, Samant MG, Felser C, Parkin SSP. 2016. Termination layer compensated tunnelling magnetoresistance in ferrimagnetic Heusler compounds with high perpendicular magnetic anisotropy. *Nat. Commun.* 7:10276
 66. Nayak AK, Nicklas M, Chadov S, Khuntia P, Shekhar C, et al. 2015. Design of compensated ferrimagnetic Heusler alloys for giant tunable exchange bias. *Nat. Mat.* 14:679
 67. Sahoo R, Wollmann L, Selle S, Höche T, Ernst B, et al. 2016. Compensated ferrimagnetic tetragonal Heusler thin films for antiferromagnetic spintronics. *Adv. Mater.* 28:8499–8504
 68. Nayak AK, Nicklas M, Chadov S, Shekhar C, Skourski Y, et al. 2013. Large zero-field cooled exchange-bias in bulk Mn_2PtGa . *Phys. Rev. Lett.* 110:127204
 69. Ryu KS, Thomas L, Yang SH, Parkin SS. 2013. Chiral spin torque at magnetic domain walls. *Nat. Nanotechnol.* 8:527–533
 70. Yang SH, Ryu KS, Parkin SS. 2015. Domain-wall velocities of up to 750 ms^{-1} driven by exchange-coupling torque in synthetic antiferromagnets. *Nat. Nanotechnol.* 10:221–226
 71. Parkin SSP, Hayashi M, Thomas L. 2008. Magnetic domain-wall racetrack memory. *Science* 320:190
 72. Schulz T, Ritz R, Bauer A, Halder M, Wagner M, et al. 2012. Emergent electrodynamics of skyrmions in a chiral magnet. *Nat. Phys.* 8:301–304
 73. Meshcheriakova O, Chadov S, Nayak AK, Rössler UK, Kübler J, et al. 2014. Large non-collinearity and spin reorientation in the novel Mn_2RhSn Heusler magnet. *Phys. Rev. Lett.* 113:087203

74. Neubauer A, Pfleiderer C, Binz B, Rosch A, Ritz R, et al. 2009. Topological Hall effect in the a phase of MnSi. *Phys. Rev. Lett.* 102:186602
75. Kanazawa N, Onose Y, Arima T, Okuyama D, Ohoyama K, et al. 2011. Large topological Hall effect in a short-period helimagnet MnGe. *Phys. Rev. Lett.* 106
76. Rana KG, Meshcheriakova O, Kübler J, Ernst B, Karel J, et al. 2016. Observation of topological Hall effect in Mn₂RhSn films. *New J. Phys.* 18:085007
77. Bernevig BA, Hughes TL, Zhang SC. 2006. Quantum spin Hall effect and topological phase transition in HgTe quantum wells. *Science* 314:1757–1761
78. König M, Wiedmann S, Brüne C, Roth A, Buhmann H, et al. 2007. Quantum spin Hall insulator state in HgTe quantum wells. *Science* 318:766–770
79. Beleanu A, Mondeshki M, Juan Q, Casper F, Felser C, Porcher F. 2011. Systematical, experimental investigations on LiMgZ (Z = P, As, Sb) wide band gap semiconductors. *J. Phys. D: Appl. Phys.* 44:475302
80. Ouardi S, Shekhar C, Fecher GH, Kozina X, Stryganyuk G, et al. 2011. Electronic structure of Pt based topological Heusler compounds with C1_b structure and "zero band gap". *Appl. Phys. Lett.* 98:211901
81. Chadov S, Qi X, Kübler J, Fecher GH, Felser C, Zhang SC. 2010. Tunable multifunctional topological insulators in ternary Heusler compounds. *Nat. Mat.* 9:541–545
82. Lin H, Wray LA, Xia Y, Xu S, Jia S, et al. 2010. Half-Heusler ternary compounds as new multifunctional experimental platforms for topological quantum phenomena. *Nat. Mat.* 9:546–549
83. Canfield PC, Thompson JD, Beyermann WP, Lacerda A, Hundley MF, et al. 1991. Magnetism and heavy fermion-like behavior in the RBiPt series. *J. Appl. Phys.* 70:5800
84. Goll G, Marz M, Hamann A, Tomanic T, Grube K, et al. 2008. Thermodynamic and transport properties of the non-centrosymmetric superconductor LaBiPt. *Physica B* 403:1065–1067
85. Fisk Z, Canfield PC, Beyermann WP, Thompson JD, Hundley MF, et al. 1991. Massive electron state in YbBiPt. *Phys. Rev. Lett.* 67:3310–3313
86. Butch NP, Syers P, Kirshenbaum K, Hope AP, Paglione J. 2011. Superconductivity in the topological semimetal YPtBi. *Phys. Rev. B* 84:220504
87. Müchler L, Casper F, Yan B, Chadov S, Felser C. 2013. Topological insulators and thermoelectric materials. *Phys. Stat. Sol. RRL* 7:91–100
88. Weng H, Fang C, Fang Z, Bernevig BA, Dai X. 2015. Weyl semimetal phase in noncentrosymmetric transition-metal monophosphides. *Phys. Rev. X* 5:011029
89. Shekhar C, Nayak AK, Sun Y, Schmidt M, Nicklas M, et al. 2015. Extremely large magnetoresistance and ultrahigh mobility in the topological Weyl semimetal candidate NbP. *Nat. Phys.* 11:645–649
90. Huang X, Zhao L, Long Y, Wang P, Chen D, et al. 2015. Observation of the chiral-anomaly-induced negative magnetoresistance in 3D Weyl semimetal TaAs. *Phys. Rev. X* 5:031023
91. Ciudad D. 2015. Weyl fermions: Massless yet real. *Nat. Mat.* 14:863–863
92. Xu SY, Belopolski I, Alidoust N, Neupane M, Bian G, et al. 2015. Discovery of a Weyl fermion semimetal and topological Fermi arcs. *Science* 349:613–617
93. Huang SM, Xu SY, Belopolski I, Lee CC, Chang G, et al. 2015. A Weyl fermion semimetal with surface Fermi arcs in the transition metal monophosphide TaAs class. *Nat. Commun.* 6:7373
94. Xu SY, Alidoust N, Belopolski I, Yuan Z, Bian G, et al. 2015. Discovery of a Weyl fermion state with Fermi arcs in niobium arsenide. *Nat. Phys.* 11:748–754
95. Xu SY, Belopolski I, Sanchez DS, Zhang C, Chang G, et al. 2015. Experimental discovery of a topological Weyl semimetal state in TaP. *Sci. Adv.* 1:e1501092–e1501092
96. Xiong J, Kushwaha SK, Liang T, Krizan JW, Hirschberger M, et al. 2015. Evidence for the chiral anomaly in the Dirac semimetal Na₃Bi. *Science* 350:413–416
97. Dai X. 2015. Weyl semimetals: A group family picture. *Nat. Mat.* 15:5–6
98. Liu ZK, Yang LX, Sun Y, Zhang T, Peng H, et al. 2015. Evolution of the Fermi surface of

- Weyl semimetals in the transition metal pnictide family. *Nat. Mat.* 15:27–31
99. Batabyal R, Morali N, Avraham N, Sun Y, Schmidt M, et al. 2016. Visualizing weakly bound surface Fermi arcs and their correspondence to bulk Weyl fermions. *Sci. Adv.* 2:e1600709–e1600709
 100. Chang G, Xu SY, Sanchez DS, Huang SM, Lee CC, et al. 2016. A strongly robust type II Weyl fermion semimetal state in Ta₃S₂. *Sci. Adv.* 2:e1600295–e1600295
 101. Lee CC, Xu SY, Huang SM, Sanchez DS, Belopolski I, et al. 2015. Fermi surface interconnectivity and topology in Weyl fermion semimetals TaAs, TaP, NbAs, and NbP. *Phys. Rev. B* 92:235104
 102. Chang G, Xu SY, Zheng H, Lee CC, Huang SM, et al. 2016. Signatures of Fermi arcs in the quasiparticle interferences of the Weyl semimetals TaAs and NbP. *Phys. Rev. Lett.* 116:066601
 103. Belopolski I, Xu SY, Sanchez DS, Chang G, Guo C, et al. 2016. Criteria for directly detecting topological fermi arcs in Weyl semimetals. *Phys. Rev. Lett.* 116:066802
 104. Yang FY. 1999. Large magnetoresistance of electrodeposited single-crystal bismuth thin films. *Science* 284:1335–1337
 105. Xu R, Husmann A, Rosenbaum TF, Saboungi ML, Enderby JE, Littlewood PB. 1997. Large magnetoresistance in non-magnetic silver chalcogenides. *Nature* 390:57–60
 106. Ali MN, Xiong J, Flynn S, Tao J, Gibson QD, et al. 2014. Large, non-saturating magnetoresistance in WTe₂. *Nature* 514:205–208
 107. Liu Z, Yang L, Wu SC, Shekhar C, Jiang J, et al. 2016. Observation of unusual topological surface states in *half*-Heusler compounds *LnPtBi* (*Ln* = Lu, Y). *arXiv:1602.05633*
 108. Hirschberger M, Kushwaha S, Wang Z, Gibson Q, Liang S, et al. 2016. The chiral anomaly and thermopower of Weyl fermions in the *half*-Heusler GdPtBi. *Nat. Mat.*
 109. Kreyssig A, Kim MG, Kim JW, Pratt DK, Sauerbrei SM, et al. 2011. Magnetic order in GdBiPt studied by x-ray resonant magnetic scattering. *Phys. Rev. B* 84:220408
 110. Müller RA, Lee-Hone NR, Lapointe L, Ryan DH, Pereg-Barnea T, et al. 2014. Magnetic structure of GdBiPt: A candidate antiferromagnetic topological insulator. *Phys. Rev. B* 90:041109
 111. Müller RA, Desilets-Benoit A, Gauthier N, Lapointe L, Bianchi AD, et al. 2015. Magnetic structure of the antiferromagnetic *half*-Heusler compound NdBiPt. *Phys. Rev. B* 92:184432
 112. Shekhar C, Nayak AK, Singh S, Kumar N, Wu SC, et al. 2016. Observation of chiral magnetotransport in *RPtBi* topological Heusler compounds. *arXiv:1604.01641*
 113. Nagaosa N, Sinova J, Onoda S, MacDonald AH, Ong NP. 2010. Anomalous Hall effect. *Rev. Mod. Phys.* 82:1539–1592
 114. Fang Z, Nagaosa N, Takahashi KS, Asamitsu A, Mathieu R, et al. 2003. The anomalous Hall effect and magnetic monopoles in momentum space. *Science* 302:92–95
 115. Kübler J, Felser C. 2012. Berry curvature and the anomalous Hall effect in Heusler compounds. *Phys. Rev. B* 85:012405
 116. Vidal EV, Stryganyuk G, Schneider H, Felser C, Jakob G. 2011. Exploring Co₂MnAl Heusler compound for anomalous Hall effect sensors. *Appl. Phys. Lett.* 99:132509
 117. Husmann A, Singh LJ. 2006. Temperature dependence of the anomalous Hall conductivity in the Heusler alloy Co₂CrAl. *Phys. Rev. B* 73:172417
 118. Wang Z, Vergniory M, Kushwaha S, Hirschberger M, Chulkov EV, et al. 2016. Time-reversal breaking Weyl fermions in magnetic Heuslers. *arXiv:1603.00479*
 119. Chang G, Xu SY, Zheng H, Singh B, Hsu CH, et al. 2016. Room-temperature magnetic topological semimetal state in half-metallic Heusler Co₂TiX (*X* = Si, Ge, or Sn). *arXiv:1603.01255*
 120. Nagamiya T, Tomiyoshi S, Yamaguchi Y. 1982. Triangular spin configuration and weak ferromagnetism of Mn₃Sn and Mn₃Ge. *Solid State Commun.* 42:385–388
 121. Tomiyoshi S, Yamaguchi Y, Nagamiya T. 1983. Triangular spin configuration and weak ferromagnetism of Mn₃Ge. *J. Magn. Magn. Mater.* 31-34:629–630
 122. Yamada N, Sakai H, Mori H, Ohoyama T. 1988. Magnetic properties of ϵ -Mn₃Ge. *Physica B+C* 149:311–315

123. Qian JF, Nayak AK, Kreiner G, Schnelle W, Felser C. 2014. Exchange bias up to room temperature in antiferromagnetic hexagonal Mn_3Ge . *J. Phys. D: Appl. Phys.* 47:305001
124. Zhang D, Yan B, Wu SC, Kübler J, Kreiner G, et al. 2013. First-principles study of the structural stability of cubic, tetragonal and hexagonal phases in Mn_3Z ($Z = \text{Ga}, \text{Sn}$ and Ge) Heusler compounds. *J. Phys.: Condens. Matter* 25:206006
125. Chen H, Niu Q, MacDonald AH. 2014. Anomalous Hall effect arising from noncollinear antiferromagnetism. *Phys. Rev. Lett.* 112:017205
126. Kübler J, Felser C. 2014. Non-collinear antiferromagnets and the anomalous Hall effect. *EPL* 108:67001
127. Nayak AK, Fischer JE, Sun Y, Yan B, Karel J, et al. 2016. Large anomalous Hall effect driven by a nonvanishing Berry curvature in the noncolinear antiferromagnet Mn_3Ge . *Sci. Adv.* 2
128. Nakatsuji S, Kiyohara N, Higo T. 2015. Large anomalous Hall effect in a non-collinear antiferromagnet at room temperature. *Nature* 527:212–215
129. Wurmehl S, Fecher GH, Kandpal HC, Ksenofontov V, Felser C, et al. 2005. Geometric, electronic, and magnetic structure of Co_2FeSi : Curie temperature and magnetic moment measurements and calculations. *Phys. Rev. B* 72:184434
130. Jungwirth T, Marti X, Wadley P, Wunderlich J. 2016. Antiferromagnetic spintronics. *Nat. Nanotechnol.* 11:231–241